MCB
Journals.ASM.org

# The FBXO4 Tumor Suppressor Functions as a Barrier to Braf$^{V600E}$-Dependent Metastatic Melanoma

**Eric K. Lee,[a,b] Zhaorui Lian,[a,b] Kurt D'Andrea,[c] Richard Letrero,[c] WeiQi Sheng,[g] Shujing Liu,[d] J. Nathaniel Diehl,[a] Dariusz Pytel,[a,b] Olena Barbash,[a,b] Lynn Schuchter,[e] Ravi Amaravaradi,[e] Xiaowei Xu,[d] Meenhard Herlyn,[f] Katherine L. Nathanson,[c,e] J. Alan Diehl[a,b,e]**

The Leonard and Madlyn Abramson Family Cancer Research Institute,[a] Department of Cancer Biology,[b] Department of Medicine,[c] Department of Pathology and Laboratory Medicine,[d] and Abramson Cancer Center,[e] University of Pennsylvania, Philadelphia, Pennsylvania, USA; The Wistar Institute, Philadelphia, Pennsylvania, USA[f]; Department of Pathology, Shanghai Cancer Center, Fudan University, Shanghai, China[g]

**Cyclin D1–cyclin-dependent kinase 4/6 (CDK4/6) dysregulation is a major contributor to melanomagenesis. Clinical evidence has revealed that p16$^{INK4A}$, an allosteric inhibitor of CDK4/6, is inactivated in over half of human melanomas, and numerous animal models have demonstrated that p16$^{INK4A}$ deletion promotes melanoma. FBXO4, a specificity factor for the E3 ligase that directs timely cyclin D1 proteolysis, has not been studied in melanoma. We demonstrate that Fbxo4 deficiency induces Braf-driven melanoma and that this phenotype depends on cyclin D1 accumulation in mice, underscoring the importance of this ubiquitin ligase in tumor suppression. Furthermore, we have identified a substrate-binding mutation, *FBXO4* I377M, that selectively disrupts cyclin D1 degradation while preserving proteolysis of the other known FBXO4 substrate, TRF1. The I377M mutation and Fbxo4 deficiency result in nuclear accumulation of cyclin D1, a key transforming neoplastic event. Collectively, these data provide evidence that FBXO4 dysfunction, as a mechanism for cyclin D1 overexpression, is a contributor to human malignancy.**

Despite recent advances in immunotherapy and targeted therapy, metastatic melanoma remains an intractable, malignant disease with limited therapeutic options. The most widely appreciated genetic insult associated with melanoma is the constitutive activation of BRAF, a consequence of a valine-to-glutamate substitution at codon 600 (BRAF$^{V600E}$) (1–3). The importance of BRAF activation is underscored by its presence in roughly half of all cutaneous melanomas (4) and by the impressive cytotoxicity and tumor regression observed in melanoma patients receiving the BRAF kinase inhibitor vemurafenib (5–7).

Attempts to model melanoma initially revealed that BRAF$^{V600E}$ expression in primary melanocytes elicits oncogene-induced senescence (8–10), as opposed to malignant growth. Consistently, ~80% of benign human nevi harbor BRAF$^{V600E}$ and never progress to melanoma (4). Thus, while BRAF-driven signaling may be an integral component of melanomagenesis, cooperation with other genetic insults is necessary.

Multiple independent lines of evidence indicate that the loss of p16$^{INK4A}$, an allosteric inhibitor of cyclin-dependent kinase 4/6 (CDK4/6)–cyclin D, cooperates with RAS-RAF to induce melanoma (11–17). These oncogenic events are clinically significant, as p16$^{INK4A}$ is commonly inactivated in melanomas (18, 19). In addition to p16$^{INK4A}$, the cyclin D1 gene (*CCND1*) is amplified in multiple melanoma subtypes (over 40% of acral melanomas) (20), also contributing to dysregulated CDK4/cyclin D1 activity.

While amplification events contribute to increased cyclin D1 expression, roughly 20% of melanomas overexpressing cyclin D1 do not exhibit genetic alterations in *CCND1* (20). The latter observation suggests that dysregulated posttranslational control may contribute to cyclin D1 overexpression. However, the role of the degradation machinery for cyclin D1, a highly labile protein (21), has not been extensively studied outside the context of a few select malignancies. Specifically, the functional status of FBXO4, the specificity factor of the SCF$^{Fbxo4}$ E3 ligase that directs polyubiquitylation of the phosphorylated cyclin D1 (22, 23), has not been examined in melanoma.

Fbxo4 belongs to a superfamily of F-box proteins, which function as substrate specificity factors for Skp1–Cul1–F-box (SCF) ubiquitin ligase complexes (24, 25). Importantly, Fbxo4 deficiency leads to nuclear accumulation of cyclin D1, which in turn promotes cyclin D1-dependent cellular transformation (23, 26, 27). The role for FBXO4 as a tumor suppressor is also supported by evidence from clinical samples; inactivating mutations in *FBXO4* have been identified in human esophageal cancers and breast cancers, with consequently elevated cyclin D1 levels (28, 29). Supporting a role for Fbxo4 as a bona fide tumor suppressor, *Fbxo4*-deficient mice develop a spectrum of tumor phenotypes, most commonly lymphoma (23).

In order to assess the impact of Fbxo4 ablation on melanomagenesis, we generated Fbxo4-deficient transgenic mice in the context of inducible Braf$^{V600E}$ activation. These genetic perturbations reveal a striking phenotype that mimics human disease. We also investigated the occurrence of *FBXO4* mutations in human melanomas and identified one mutation, I377M, that selectively

**Received** 5 June 2013 **Returned for modification** 24 June 2013
**Accepted** 31 August 2013
**Published ahead of print** 9 September 2013

Address correspondence to J. Alan Diehl, adiehl@mail.med.upenn.edu.

This paper is dedicated in fond memory to Patricia Lorenzo, a former member of the Molecular Oncogenesis NCI study section and the University of Hawaii Cancer Center, who brightened deliberations with her compassion, affability, and dedication. Her remarkable courage in the face of terminal cancer has been inspirational.

Supplemental material for this article may be found at http://dx.doi.org/10.1128/MCB.00706-13.



doi:10.1128/MCB.00706-13

inactivates $SCF^{Fbxo4}$ ubiquitin ligase activity toward cyclin D1 but not the other known substrate, TRF1.

## MATERIALS AND METHODS

**Cell culture, transfections, and plasmids.** 293T and mouse embryonic fibroblasts (MEFs) were maintained in Dulbecco's modified Eagle's medium (DMEM) containing glutamine, penicillin-streptomycin, and 10% fetal bovine serum (FBS) (Gemini). Mouse embryos extracted at day 14 of gestation were passaged at $3 \times 10^5$ cells every 3 days. Human melanoma cell lines were maintained in Tumor2 medium containing MCDB153–Leibovitz's L-15 medium (80/20, vol/vol), 2% FBS, 5 μg/ml insulin, 1.68 mM calcium chloride, and penicillin-streptomycin. pcDNA3 Flag-tagged FBXO4 was a gift from Michelle Pagano. pcDNA3 Myc-tagged Fbxo4 was generated as described previously (28). The pcDNA3 Flag-tagged FBXO4 mutants were generated by using a QuikChange site-directed mutagenesis kit (Stratagene) according to the manufacturer's instructions, and cDNAs were sequenced in their entirety. Cells were transfected by using Lipofectamine reagent (Invitrogen). Retroviral pBabe-puro Flag-tagged FBXO4 was used for infection of melanoma cell lines.

**Histology/immunohistochemistry.** Tissues were fixed in 10% buffered formalin overnight, followed by dehydration with ethanol, paraffin embedding, and sectioning. Immunohistochemistry (IHC) was performed on 5- to 8-μm sections, and hematoxylin and eosin (H&E) staining was performed by using standard protocols. Antibodies utilized for IHC staining were purified cyclin D1 (AB3; Calbiochem), Fbxo4 (YenZym Antibodies), phospho-S11 Fbxo4 (YenZym Antibodies), and S-100 (Dako) antibodies. Antigens were retrieved with Antigen Retrieval Citra Plus (Biogenex) by boiling for 10 min, and antibodies were visualized with a Vectastain ABC Elite kit (Vector Laboratories) and a peroxidase substrate kit (Vector Laboratories).

**Immunoprecipitation and Western analysis.** Cells were harvested in Tween 20 buffer (50 mM HEPES [pH 8.0], 150 mM NaCl, 2.5 mM EGTA, 1 mM EDTA, 0.1% Tween 20, protease, and phosphatase inhibitors [1 mM phenylmethylsulfonyl fluoride {PMSF}, 20 U/ml aprotinin, 5 μg/ml leupeptin, 1 mM dithiothreitol {DTT}, 0.4 μM NaF, and 10 μM β-glycerophosphate]); protein concentrations of samples were determined by a Bradford assay (30). Proteins were resolved by SDS-PAGE, transferred onto nitrocellulose membranes, and analyzed by immunoblotting. Antibodies used were as follows: Fbxo4 rabbit polyclonal antibody (YenZym Antibodies), cyclin D1 mouse monoclonal antibody D1-72-13G, cyclin D1 mouse anti-human antibody (Calbiochem), ubiquitin-P4D1 (Covance), αB crystallin (Stressgen), Skp1 (Cell Signaling), M2-Flag (Sigma), 9E10-Myc (Santa Cruz), TRF1 (gift from Xuedong Liu), MAP-2 (Millipore), and Ku70 (Abcam). Antibody binding was visualized by enhanced chemiluminescence (PerkinElmer).

**Immunofluorescence.** Fbxo4-null MEFs were plated at an optimal density on glass coverslips and transfected with the wild-type (WT) FBXO4 or I377M plasmid. Forty-eight hours later, cells were fixed and permeabilized with methanol-acetone (1:1). Cyclin D1 was visualized as described previously (28).

**Experimental animals and genotyping.** Animal experiments were conducted in accordance with IACUC protocols and University Laboratory Animal Research (ULAR) guidelines. Generation of mice and genotyping protocols were described previously (23, 31). 4-Hydroxytamoxifen (4HT) was freshly prepared in dimethyl sulfoxide (DMSO) (5 mM) and applied topically for three consecutive days to postnatal day 2 pups.

**Statistical analysis.** Kaplan-Meier tumor-free survival graphs were generated and analyzed with GraphPad Prism software. Other statistical analyses utilized a two-tailed Student *t* test, with *P* values of $<0.05$ indicating statistical significance. Error bars in the figures represent the means ± the standard deviations.

**FBXO4 mutation screening.** PCR amplifications for *FBXO4* exons 1 and 7 were performed by using a Roche GC-Rich PCR system kit. The 20-μl PCR mixture included 4.2 μl of PCR-grade water, 2 μl of each 5 μM PCR primer, 4 μl of PCR buffer (vial 2), 4 μl of resolution solution (vial 3), 0.4 μl of nucleotide mix (vial 6), 0.4 μl of enzyme mix (vial 1), and 15 ng of genomic DNA (5 ng/μl). The touchdown PCR conditions were an initial cycle at 95°C for 10 min; 8 cycles at 95°C for 30 s, 61°C for 90 s, (−0.5°C/cycle), and 72°C for 60 s; 35 cycles at 95°C for 30 s, 57°C for 90 s, and 72°C for 60 s; and a final step at 72°C for 10 min. For PCR primer sequences, see Table 1.

**TABLE 1** PCR primers

| Exon | Primer sequence | |
|---|---|---|
| | Forward | Reverse |
| 1 | GGGAAGTTAATTGTTGACAGG | AACTGTAGCTTCTCGGTGAC |
| 2 | GGAATGTTTCAGGTGTTTCAG | AGGGTCAGGATTAACTTGGA |
| 3 | TGTCTGTCTATTGTTCTCCT | AGAATGTCAAGCTCAAAGTG |
| 4 | AGGACTGTTATAAGCCTTGC | CTTGTATGCTCTTCCCTTGCT |
| 5 | TCTTAGGTATTGGATCAGGAG | TAAGAAGCCACAGTAAAGTC |
| 6 | TTAAACTGTGGAGACATCTG | TCACCAATCAAATAGCTTCC |
| 7 | CCTCATACATGGAAGCAAGTC | AGCTGTCCAAATGAAAGCCT |

PCR amplifications for *FBXO4* exons 2, 3, 4, 5, and 6 were performed by using Platinum *Taq* DNA polymerase (Invitrogen). The 25-μl PCR mixture included 14.5 μl of PCR-grade water, 1.25 μl each 5 μM PCR primer, 2.5 μl 10× PCR buffer, 1 μl 50 mM $MgCl_2$, 1.25 μl of 2.5 mM deoxynucleoside triphosphate (dNTP) mix, 0.25 μl Platinum *Taq* DNA polymerase, and 15 ng of genomic DNA (5 ng/μl). The same PCR conditions as described above were used.

For sequencing on an ABI 3130 genetic analyzer, unincorporated dNTPs were first removed from PCR products by using the Affymetrix ExoSAP-IT reagent. The ExoSAP-IT reaction mixture included 5 μl of PCR product and 1 μl of ExoSAP-IT reagent. The thermal cycling conditions were 37°C for 15 min followed by 80°C for 15 min. A sequencing reaction using ABI BigDye Terminator (BDT) v1.1 cycle sequencing chemistry was performed. Ten microliters of a solution consisting of 7.4 μl of PCR-grade water, 2 μl of BDT v1.1, and 0.6 μl of the forward PCR primer (5 μM) was then added to the samples. The thermal cycling conditions for this step were an initial cycle at 95°C for 60 s and 25 cycles at 95°C for 10 s, 50°C for 5 s, and 60°C for 4 min. Following the sequencing reaction, the samples were then purified by passing them through Sephadex columns by using a centrifuge. Ten microliters of Hi-Di formamide was then added to each sample. Sequencing was then performed on the ABI 3130 genetic analyzer.

**Sequenom (iPLEX) genotyping.** Genotyping was performed for *AKT1* E17K; *AKT3* E17K; BRAF G466A/E/R/V, V600E/D/K/E/L/R, and K601E; *CDK4* K22Q and R24C/H; *CTNNB1* D32A/E/G/V, S37F/Y/DEL, and S45F/Y; *FBXO4* H364R and I377M; *GNA11* Q209L/P; *GNAQ* Q209H/L/P/R/X; *KIT* W557R, L576P, V599A/D, K642E, R634W, D816H/V, D820Y, N822I, Y823D, and A829P; *MEK1* C121S; *MEK2* F57S, Q60P, K61E/T, and L119P; *MET* Y1248H; and NRAS G12A/C/D/R/S/V, G13A/C/D/R/S/V, and Q61E/H/K/L/P/R mutations. For genotyping using the Sequenom MassArray spectrometry platform, samples were plated and sent to the Perelman School of Medicine Genomics Facility. An initial PCR amplification of the DNA was performed with a 5-μl reaction mixture consisting of 0.8 μl of high-performance liquid chromatography (HPLC)-grade water, 0.5 μl of 10× PCR buffer with 20 mM $MgCl_2$, 0.4 μl of 25 mM $MgCl_2$, 0.1 μl of 25 mM dNTP mix, 1 μl of 0.5 μM primer mix, 0.2 μl of Sequenom PCR enzyme, and 2 μl of genomic DNA (5 ng/μl). PCR conditions were an initial cycle at 94°C for 2 min; 45 cycles at 95°C for 30 s, 56°C for 30 s, and 72°C for 60 s; and a final step at 72°C for 5 min. This was followed by shrimp alkaline phosphatase (SAP) treatment of the samples with 2 μl of SAP mix consisting of 1.53 μl of HPLC-grade water, 0.17 μl of SAP buffer, and 0.3 μl of SAP enzyme. The thermal cycling conditions were 37°C for 40 min followed by 85°C for 5 min. Following SAP treatment, a single-base-pair extension reaction was performed by using Sequenom iPLEX Gold chemistry, where 2 μl of the iPLEX reaction mix was added to the samples. The reaction mix consisted of 0.62 μl of HPLC-grade water, 0.2 μl of iPLEX buffer, 0.2 μl of iPLEX terminator mix, 0.94

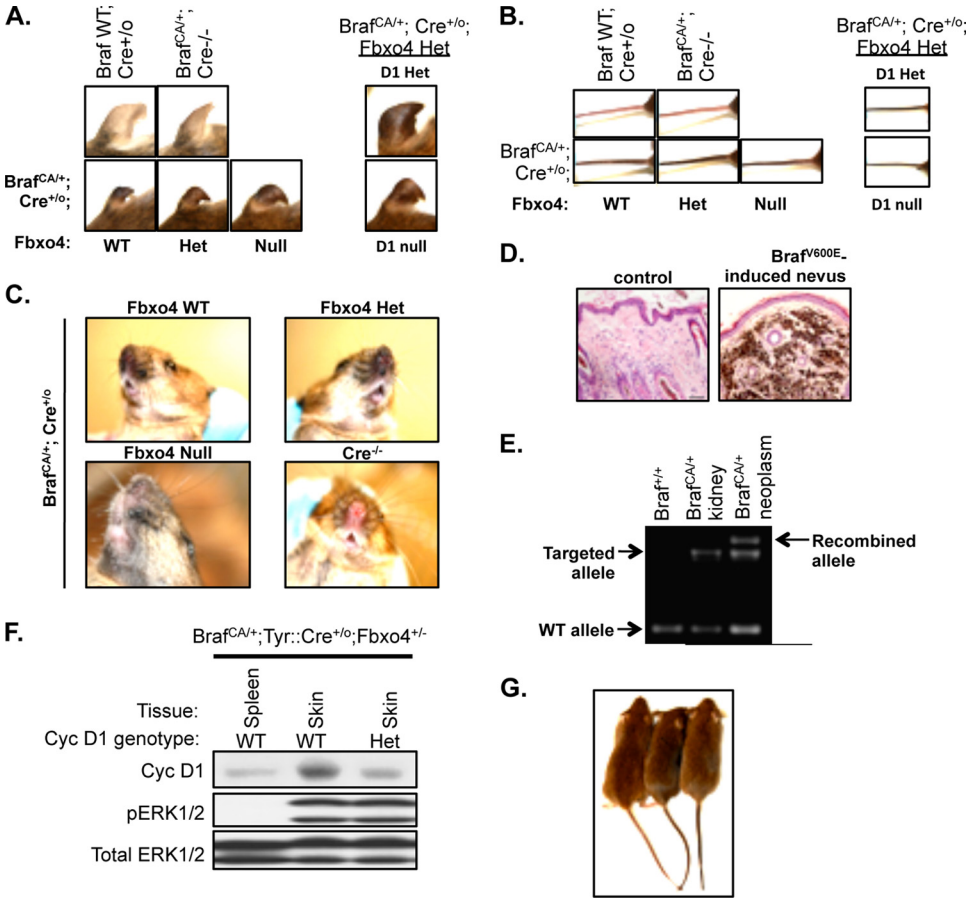


**FIG 1** Braf$^{V600E}$ drives melanocyte hyperplasia independent of Fbxo4 or cyclin D1 status. (A and B) Glabrous skin of mice with the indicated genotypes. (C) Benign hyperplastic nevi of the indicated *Fbxo4* transgenic mice on a Braf-activated background. (D) Low-power (left) and high-power (right) magnifications of nevus. (E) Amplification of DNA extracts isolated from mice/tissue of the indicated genotypes. (F) Lysates prepared from the indicated tissues/genotypes were assessed for cyclin D1, phospho-ERK1/2, and total ERK1/2 expression by Western blotting. (G) *Braf*$^{+/+}$ (left), *Braf*$^{V600E/+}$; *cycD1*$^{+/-}$ (middle), and *Braf*$^{V600E/+}$; *cycD1*$^{+/+}$ (right) mice were monitored for melanocyte hyperplasia.

μl of primer mix, and 0.04 μl of iPLEX enzyme. Thermal cycling conditions were an initial cycle at 94°C for 30 s, 40 cycles at 94°C for 5 s (52°C for 5 s and 80°C for 5 s [repeating 5 times per cycle]), and a final step at 72°C for 3 min. The samples were then resin treated and spotted onto a SpectroCHIP to be run on the Sequenom MassArray platform.

**Sample collection.** All patients from which acral and cutaneous melanomas were genotyped provided written informed consent approved by the University of Pennsylvania IRB. Also, this study was approved by the Ethical Committee for Clinical Research at the Fudan University Shanghai Cancer Center, Shanghai, China. All samples were analyzed by H&E processing for tumor amounts at the Abramson Histology Core Facility; those with tumor nuclei that were <70% of the total on the slide were marked for macrodissection. Samples with over 70% tumors had slides cut directly into Eppendorf tubes for direct DNA extraction. Those samples with <70% tumors were cut onto slides for macrodissection by using the marker H&E. DNA was extracted from formalin-fixed, paraffin-embedded samples by using standard methods.

## RESULTS

**Braf$^{V600E/+}$; Fbxo4-deficient mice develop highly aggressive melanoma.** Since cyclin D1/CDK4 dysregulation, particularly with respect to p16$^{INK4A}$ inactivation, plays a crucial role in the development of melanoma, we assessed whether a loss of the F-box component of the cyclin D1 ubiquitin ligase Fbxo4 facilitates Braf$^{V600E}$-driven melanoma. *Fbxo4*$^{-/-}$ mice (23) were intercrossed with *Braf*$^{CA/+}$; *Ty r*::*CreER*$^{+/o}$ mice (8) to generate *Braf*$^{CA/+}$; *CreER*$^{+/o}$; *Fbxo4*$^{+/-}$ and *Braf*$^{CA/+}$; *CreER*$^{+/o}$; *Fbxo4*$^{-/-}$ mice (see Fig. S1 in the supplemental material). In an effort to more closely recapitulate physiologically relevant changes in human disease, our studies were conducted with mice carrying exactly one copy of *Braf*$^{CA}$, the expression of which requires topical 4-hydroxytamoxifen (4HT) treatment in order to trigger the excision of exons 15 to 18/stop codon of wild-type *Braf* and permit the expression of an alternate fragment from exons 15 to 18 encoding the V600E mutation (31). Additionally, experimental mice inherited exactly one copy of melanocyte-specific tyrosinase promoter-driven *Tyr*::*CreER*$^{T2}$. Previous studies demonstrated that *Braf*$^{CA/+}$; *Tyr*::*CreER* mice develop melanocytic hyperplasias but do not succumb to melanoma for up to 2 years from the time of 4HT-mediated Braf activation (8). However, melanomas occur rapidly, with the concomitant loss of Pten (8), providing evidence in this mouse model that inactivation of a tumor suppressor relevant to melanoma pathogenesis cooperates with Braf$^{V600E}$ to induce oncogenic disease.

Braf$^{V600E}$ expression was induced neonatally by 4HT administration. By 3 weeks post-4HT treatment, mice of all genotypes exhibited diffusely hyperpigmented skin, most readily seen on the

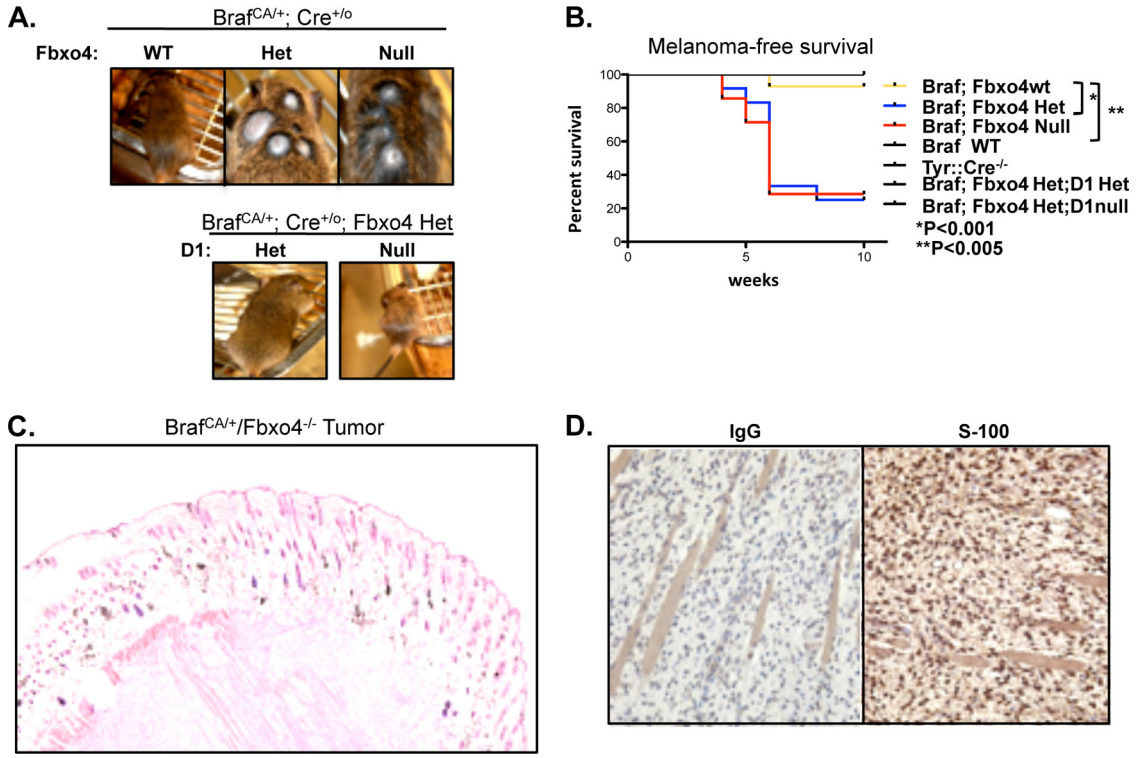


**FIG 2** Fbxo4 deficiency induces melanoma in Braf-activated mice. (A) Representative images of Braf-activated mice with the indicated *Fbxo4* status at 12 weeks post-4HT treatment. (B) Kaplan-Meier survival analysis of 4HT-treated mice ($Braf^{CA/+}$/*Tyr*::$Cre^{-/-}$, $n = 20$; $Braf^{+/+}$/*Tyr*::$Cre^{+/o}$, $n = 20$; $Braf^{CA/+}$/*Tyr*::$Cre^{+/o}$/$Fbxo4^{+/+}$, $n = 15$; $Fbxo4^{+/-}$, $n = 15$; $Fbxo4^{+/-}$, $n = 10$) (*, comparison of $Braf^{CA/+}$/*Tyr*::$Cre^{+/o}$/$Fbxo4^{+/+}$ versus $Braf^{CA/+}$/*Tyr*::$Cre^{+/o}$/$Fbxo4^{+/-}$; **, comparison of $Braf^{CA/+}$/*Tyr*::$Cre^{+/o}$/$Fbxo4^{+/+}$ versus $Braf^{CA/+}$/*Tyr*::$Cre^{+/o}$/$Fbxo4^{-/-}$). (C) Low-magnification micrograph of a $Braf^{CA/+}$/Fbxo4$^{-/-}$ tumor. Highly invasive amelanotic melanocytes infiltrate skeletal muscle. (D) S-100 neural crest-specific nuclear staining of tumor cells.

glabrous skin of the ears and tails, and with sporadic melanocytic hyperplasias around the muzzle (Fig. 1A to C). Histological analysis of a $Braf^{CA/+}$; $CreER^{+/o}$; *Fbxo4*-deficient nevus revealed neoplastic expansion of melanocytes, which are identified by naturally pigmented cells in the dermis of H&E-stained cutaneous sections and normally confined to murine hair follicles (Fig. 1D). Importantly, both $Braf^{+/+}$; $CreER^{+/o}$ and $Braf^{CA/+}$; $CreER^{-/-}$ mice had unaffected skin and failed to develop any phenotype throughout the duration of our study, indicating that our observations are critically dependent on $CreER^{T2}$-mediated induction of $Braf^{V600E}$. Excision of wild-type exons 15 to 18 was confirmed in DNA extracts from melanotic neoplasms (Fig. 1E). Of note, $Braf^{V600E}$ expression was detected only in neoplasms and tumors, whereas non-tyrosinase-expressing tissue, such as the kidney, did not undergo Braf allelic recombination.

To definitively address the dependence of Fbxo4-mediated tumorigenicity on cyclin D1, we also crossed $Braf^{CA/+}$; $CreER^{+/o}$; *Fbxo4*-deficient mice with cyclin D1 knockout mice (32). Because complete cyclin D1 deletion (homozygous null) may impact the oncogenic signals induced by activated Braf, we compared the melanoma-free survivals of $Braf^{CA/+}$; $CreER^{+/o}$; $Fbxo4^{+/-}$; $Ccnd1^{+/+}$ mice and $Braf^{CA/+}$; $CreER^{+/o}$; $Fbxo4^{+/-}$; $Ccnd1^{+/-}$ mice. In lysates prepared from pretumorigenic skin tissue, cyclin D1 expression was correlated with gene dosage (Fig. 1F, lane 2 versus lane 3), although mutational activation of Braf, confirmed by tissue-specific phospho-ERK1/2 signaling, also enhanced cyclin D1 expression relative to control tissue (Fig. 1F, lane 1 versus lanes 2 and 3). However, cyclin D1 levels, as governed by gene dosage, had no noticeable effect on the latency associated with detection of melanocyte hyperproliferation (Fig. 1A, B, and G).

At 4 to 6 weeks post-4HT administration, $Braf^{CA/+}$; $CreER^{+/o}$; $Fbxo4^{+/-}$ and $Braf^{CA/+}$; $CreER^{+/o}$; $Fbxo4^{-/-}$ mice developed numerous rapidly growing tumors, while $Braf^{CA/+}$; $CreER^{+/o}$; $Fbxo4^{+/+}$ mice, in the absence of further genetic manipulation, remained tumor free (Fig. 2A). Pathologically, tumors of $Braf^{CA/+}$; $CreER^{+/o}$; *Fbxo4*-deficient mice were cutaneous oligomelanotic masses appearing on dorsal and ventral surfaces with associated alopecia. Over 60% of $Braf^{CA/+}$; $CreER^{+/o}$; *Fbxo4*-deficient mice developed tumors within 2 months (Fig. 2B), while one $Braf^{CA/+}$; $Fbxo4^{+/+}$; $CreER^{+/o}$ mouse developed tumors at 6 weeks post-4HT treatment albeit with a reduced tumor burden (see Fig. S2A in the supplemental material).

If *Fbxo4*-deficient tumorigenesis is dependent upon cyclin D1 accumulation, we expected that genetic manipulation of cyclin D1 expression would impact the tumor burden of $Braf^{CA/+}$; $CreER^{+/o}$; *Fbxo4*-deficient mice. Remarkably, reduction of cyclin D1 expression by deletion of one allele was sufficient to completely abolish tumor development on a $Braf^{CA/+}$; $CreER^{+/o}$; *Fbxo4*-deficient background (Fig. 2B).

Cross sections of $Braf^{CA/+}$; $CreER^{+/o}$; *Fbxo4*-deficient tumors revealed rapidly proliferating, highly invasive, mixoid epitheloid spindle cells infiltrating skeletal muscle (Fig. 2C). Immunohistochemistry for nuclear S-100 neural crest-specific

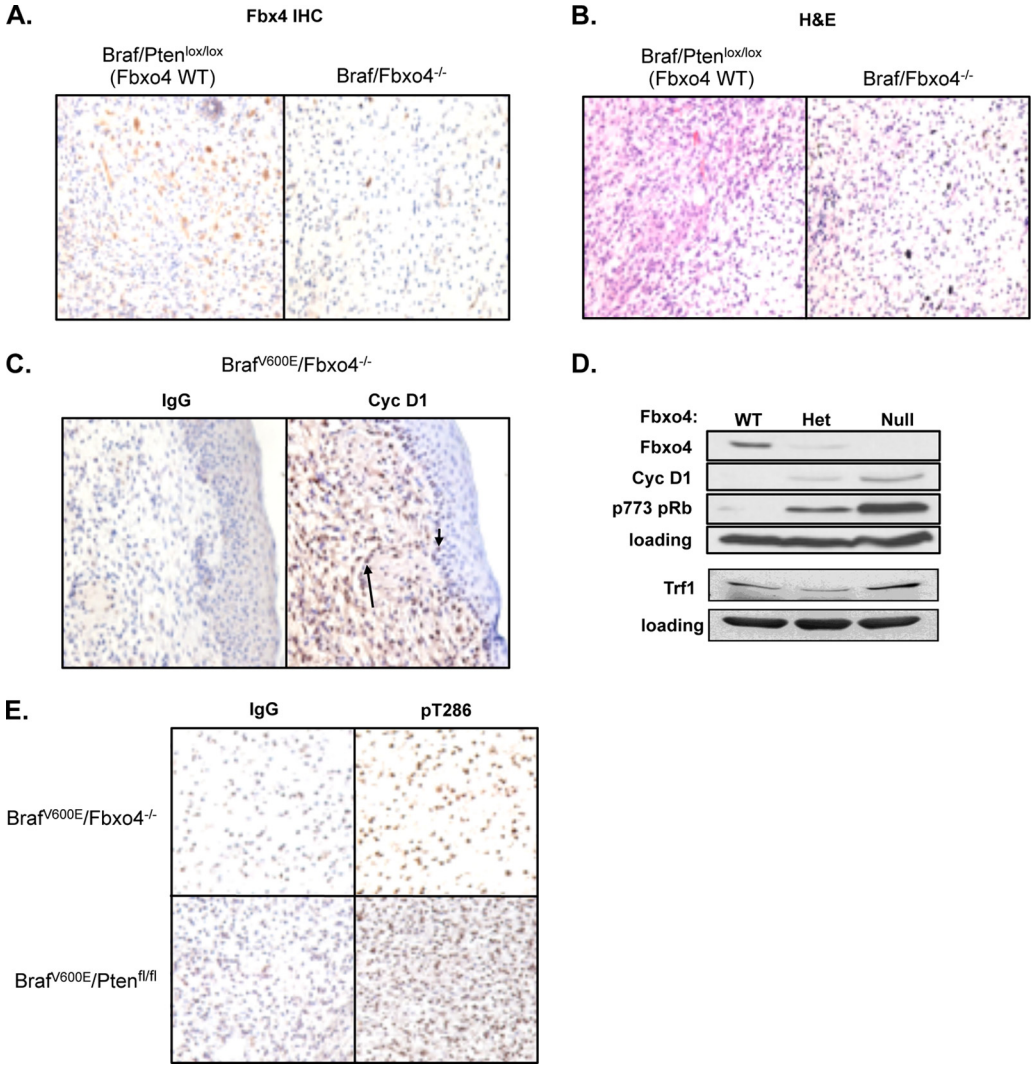


**FIG 3** Cyclin D1 accumulates in *Braf*$^{V600E}$*/Fbxo4*-deficient tumors. (A and B) Fbxo4 immunohistochemistry (A) and hematoxylin and eosin staining (B) of *Braf*$^{V600E}$*/Fbxo4*$^{-/-}$ tumor sections. (C) Cyclin D1 immunohistochemistry of paraffin-embedded tumor sections derived from *Braf*$^{V600E}$*/Fbxo4*-deficient mice. Arrows indicate intense nuclear cyclin D1 staining. Arrow indicate cyclin D1 expression in the mitotic layer of the epidermis. Note the relative intensities and the absence of cyclin D1 in the postmitotic layer of the epidermis. (D) Western analysis of the indicated proteins isolated from tumor lysates of *Braf*$^{V600E}$*/Fbxo4* WT, heterozygous (Het), or null mice. (E) Phospho-T286 cyclin D1-specific immunohistochemistry of *Braf*$^{V600E}$*/Fbxo4*-deficient tumors.

staining and Melan-A confirmed the melanocytic origin of the tumor cells (Fig. 2D; see also Fig. S2B in the supplemental material) (33, 34). Evidence of lymphogenous spread was routinely observed in tumor-bearing mice, as lymph nodes were grossly pigmented. Histologic evidence of metastases was observed in the lung, brain, and bone (see Fig. S2C to E in the supplemental material).

**Nuclear accumulation of cyclin D1 in Braf$^{V600E}$-driven melanomas.** To verify Fbxo4 loss in *Braf*$^{CA/+}$; *CreER*$^{+/o}$; *Fbxo4*$^{-/-}$ tissue, we performed immunohistochemistry, utilizing *Braf*$^{CA/+}$; *CreER*$^{+/o}$; *Pten*$^{lox/lox}$ melanomas for comparison (8). Fbxo4 was undetectable in *Braf*$^{CA/+}$; *CreER*$^{+/o}$; *Fbxo4*$^{-/-}$ tumors (Fig. 3A; see also Fig. S3A in the supplemental material). We noted that tumors derived from *Fbxo4*$^{-/-}$ and *Pten*$^{lox/lox}$ mice were histopathologically indistinguishable (Fig. 3B; see also Fig. S3B). Immunohistochemical analysis of tumor sections revealed nuclear accumulation of cyclin D1 in tumors (Fig. 3C; see also Fig. S3C). We also confirmed cyclin D1 accumulation and phosphorylation of retinoblastoma (Rb) at S773 (Fig. 3D) by Western analysis. Tumors also exhibited nuclear accumulation of phospho-T286 (Fig. 3E). These results suggest that *Fbxo4* deficiency accelerates melanoma in Braf-activated animals and leads to dysregulation of cyclin D1.

**Identification of FBXO4 mutations in human melanoma.** In light of the observation that up to 20% of human melanomas with cyclin D1 overexpression lack genetic perturbations at the *CCND1* locus (20), we investigated the prevalence of mutations within the complete *FBXO4* gene in 37 cell lines from the Wistar Melanoma Collection. We identified one point mutation, c.T1131G, which results in a single-amino-acid substitution in which isoleucine 377 is replaced by methionine (p.I377M) at a frequency of 8% (see Table S1 in the supplemental material). An additional 111 melanoma cell lines were evaluated by Sequenom analysis specifically for *FBXO4* c.T1131G; two additional cell lines carrying p.I377M

**TABLE 2** Recurrent FBXO4 I377M mutations in human melanoma cell lines[a]

| Sample identification | Origin | Type of melanoma | BRAF | NRAS | KIT | FBX04 nucleotide | FBX04 protein | Zygosity | SIFT | Polyphen2 | Other mutation |
|---|---|---|---|---|---|---|---|---|---|---|---|
| TB4286DZ1 | Tumor | Cutaneous | WT | WT | WT | c.T1131G | p.I377 M | Heterozygous | 0.04 | 0.868 | |
| WM793 | Cell line | VGP | p.V600E | WT | WT | c.T1131G | p.I377 M | Homozygous | 0.04 | 0.868 | CDK4-K22Q |
| 1205Lu | Cell line | Cutaneous metastatic | p.V600E | WT | WT | c.T1131G | p.I377 M | Homozygous | 0.04 | 0.868 | CDK4-K22Q |
| WM115 | Cell line | Lymph node | p.V600E | WT | WT | c.T1131G | p.I377 M | Heterozygous | 0.04 | 0.868 | |
| WM2090 | Cell line | Cutaneous metastatic | p.V600E | WT | WT | c.T1131G | p.I377 M | Heterozygous | 0.04 | 0.868 | |
| WM3918 | Cell line | Cutaneous metastatic | WT | WT | WT | c.T1131G | p.I377 M | Heterozygous | 0.04 | 0.868 | $NF1^{-/-}$ |
| WM3523 | Cell line | Cutaneous metastatic | p.V600E | WT | WT | c.A1037G | p.H346R | Heterozygous | 0.08 | 0.987 | |
| 2005_02233 | Tumor | Primary mucosal | WT | WT | WT | c.G653C | p.G218A | Heterozygous | 0.01 | 0.998 | |
| 2009_20387 | Tumor | Primary mucosal | WT | WT | WT | c.T665C | p.S219P | Heterozygous | 0.01 | 0.995 | |
| 2003_07702 | Tumor | Primary mucosal | WT | WT | WT | c.C959T | p.S320F | Heterozygous | 0.02 | 0.995 | |

[a] A single-nucleotide substitution in *FBXO4* exon 7 was identified in five melanoma cell lines by either Sequenom analysis or the ABI 3130 genetic analyzer. Four of these five cell lines exhibited a concurrent Braf mutation. VGP, vertical growth phase; SIFT, scale-invariant feature transform; Polyphen2, polymorphism phenotyping version 2.

were identified. Thus, this mutation was found in five cell lines and four independent clones (Table 2; see also Fig. S4 in the supplemental material). p.I377M was present in cell lines from both radial and vertical growth phases as well as metastatic lesions, suggesting that the substitution is an early neoplastic event. Complete sequencing of *FBXO4* in 39 cutaneous, 7 acral, and 15 mucosal melanomas revealed p.I377M in a primary cutaneous tumor as well as additional point mutants in the C-terminal, substrate-binding region (see Table S2 in the supplemental material). The I377M mutation was reported once in 1/4,512 alleles (0.0002%) in 1000Genomes. The majority of residues targeted, including I377, are highly conserved among metazoans (35) (see Fig. S5B in the supplemental material). Notably, while previous studies established inactivating FBXO4 mutations in the 14-3-3ϵ-dependent dimerization domain in human esophageal cancer (28, 36), we detected no such mutations in melanoma, suggesting that differential selection pressures exist in different tumor types, resulting in distinct mechanisms of FBXO4 dysfunction (see Fig. S5A and C).

**The FBXO4 I377M mutant exhibits impaired cyclin D1 recruitment and ubiquitylation.** The location of the I377M mutation suggested that it could potentially alter substrate recognition by FBXO4. Isoleucine 377 is located within an α-helix (α-helix E) at the C-terminal tail of the substrate-binding domain (see Fig. S5A in the supplemental material). Further support for this stems from available crystallographic data indicating that α-helix E is solvent accessible and resides adjacent to but outside the FBXO4-TRF1 substrate interface; we considered the possibility that the I377M mutation retains the ability to regulate TRF1 (35, 37) while losing its ability to regulate cyclin D1. We therefore assessed the impact of the I377M mutation on the regulation of both cyclin D1 and TRF1. Because FBXO4-dependent recruitment of cyclin D1 depends on αB crystallin as a cofactor, we also assessed αB crystallin association with the FBXO4 I377M mutant. FBXO4, αB crystallin, and cyclin D1/CDK4 were expressed in 293T cells; to facilitate binding, we inhibited cyclin D1 degradation with MG132. FBXO4 was immunoprecipitated, and the association with cyclin D1/αB crystallin was assessed. Although the FBXO4 I377M mutant exhibited a significantly impaired association with both cyclin D1 and αB crystallin (Fig. 4A), no defect in binding to TRF1 was observed (Fig. 4B), indicating that global protein folding was unaffected and that unique substrate-binding interfaces exist (37, 38). Conversely, FBXO4 mutations within the established FBXO4-TRF1 interface (α-helix D, residues 340 to 352 [37, 38]) had no detectable effect on cyclin D1/αB crystallin recruitment but disrupted binding to TRF1 (Fig. 4A and B). These findings provide evidence for a paradigm in which tumor cells expressing the *FBXO4* I377M mutation can maintain surveillance of TRF1 and possibly other unidentified substrates while selectively permitting dysregulation of cyclin D1. Consistent with the I377M mutation disrupting FBXO4-cyclin D1 binding, FBXO4 was not recovered efficiently in cyclin D1 complexes isolated from melanoma cell lines harboring the FBXO4 I377M mutant (Fig. 4C).

To further resolve the interface responsible for interactions with cyclin D1, we made point mutations within α-helix E of FBXO4 and assessed binding to cyclin D1. Our analysis revealed a role for E379 in FBXO4 binding to cyclin D1 (see Fig. S5D and E in the supplemental material). In addition, we also entertained the possibility that the FBXO4 I377M mutant disrupts FBXO4 dimerization itself, given evidence that FBXO4 can self-associate in an antiparallel fashion (35); wild-type myc-FBXO4 was coexpressed with Flag-FBXO4 mutants, and complexes were isolated by immunoprecipitation. Critically, the FBXO4 I377M and H346R mutants retained full dimerization potential (see Fig. S5F). Thus, mutation of residues that mediate either cyclin D1 (I377) or TRF1 (H346) binding does not impact FBXO4 dimerization.

**Cyclin D1 is refractory to FBXO4 I377M-dependent regulation.** We subsequently determined if impaired substrate recognition results in a defect in substrate ubiquitylation. FBXO4, αB crystallin, and cyclin D1/Cdk4 were expressed in 293T cells; ubiquitin-conjugated proteins were isolated by using a ubiquitin-specific antibody; and the presence of ubiquitylated cyclin D1 was assessed by immunoblotting. Strikingly, the FBXO4 I377M mutant possessed undetectable cyclin D1-ubiquitylating activity, while wild-type Fbxo4 triggered robust cyclin D1 ubiquitylation (Fig. 5A). We also investigated the capacity of melanoma cells that harbor endogenous *FBXO4* I377M mutations to ubiquitylate cyclin D1. Human melanoma 451Lu and 1205Lu cells (wild-type and I377M mutant *FBOX4*, respectively) were subjected to proteasome inhibition and probed for ubiquitylated cyclin D1. Cyclin D1 ubiquitylation was markedly decreased in cells harboring the mutation (Fig. 5B). In contrast, no decrease in Trf1 polyubiquitylation was observed (Fig. 5B).

Because the I377M mutation impairs FBXO4-mediated cyclin D1 ubiquitylation, we anticipated that cyclin D1 should accumulate in cells harboring the FBXO4 I377M mutation; we thus com-

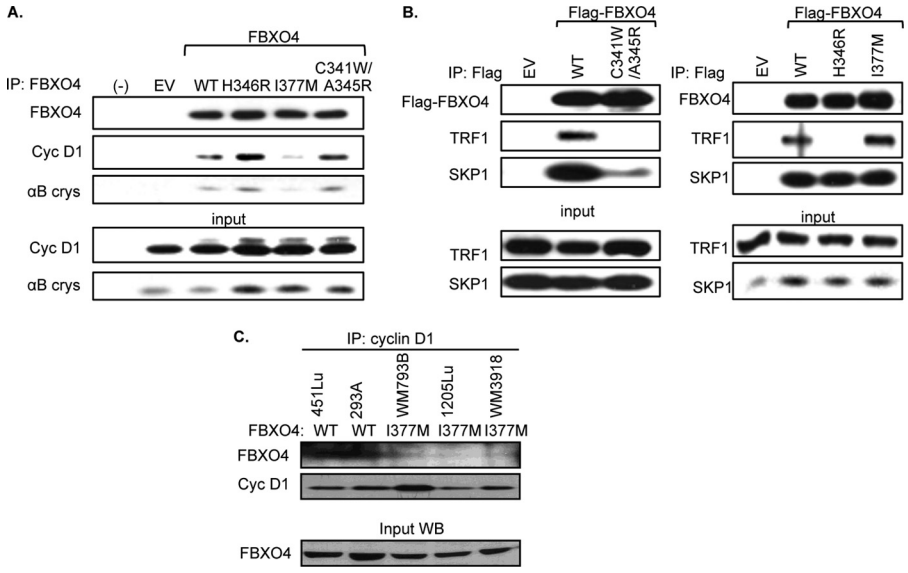


**FIG 4** Distinct Fbxo4 substrate-binding domain mutants selectively disrupt recruitment of different substrates. (A) 293T cells overexpressing Fbxo4, αB crystallin, and cyclin D1/CDK4 were subjected to MG132 proteasomal inhibition. Fbxo4 was immunoprecipitated from lysates and assessed for substrate/cofactor binding. EV, empty vector. (B) Cell extracts prepared from 293T cells expressing Fbxo4 and TRF1 and treated with MG132 proteasomal inhibition were subjected to immunoprecipitation (IP) for Fbxo4, and substrate binding was assessed by immunoblotting. (C) Lysates prepared from the indicated cells treated with MLN9708 to inhibit SCF function and stabilize SCF-cyclin complexes were subjected to precipitation with a cyclin D1-specific monoclonal antibody (top and middle) or were subjected to direct Western blotting (WB) (bottom). Lysates resolved by SDS-PAGE were transferred onto membranes and blotted with the indicated antibodies.

pared melanoma cell lines containing wild-type FBXO4 with and without cyclin D1 amplification. Immunoblotting revealed robust cyclin D1 accumulation in cells harboring the FBXO4 I377M mutation (Fig. 5C). Strikingly, cyclin D1 accumulation in FBXO4 mutant lines paralleled or exceeded that observed in cells containing CCND1 amplification (Fig. 5C, compare lane 1 to lanes 4 to 6). Notably, TRF1 levels were unaffected by the presence of the FBXO4 I377M mutation. Quantification of cyclin D1 mRNA from the same cells revealed no correlation with cyclin D1 protein accumulation (Fig. 5D).

If FBXO4 represents a rate-limiting determinant of cyclin D1 regulation, reconstitution of wild-type FBXO4 in cells should restore cyclin D1 regulation in FBXO4 I377M cells. To test this notion, cells were stably infected with a retrovirus encoding either wild-type FBXO4, the FBXO4 I377M mutant, or green fluorescent protein (GFP). Consistently, cyclin D1 expression was reduced only by wild-type FBXO4 (Fig. 5E). Importantly, α-helix D C341W/A345R mutants retained full ubiquitylating capacity (Fig. 5F), consistent with α-helix E mediating cyclin D1 recognition and α-helix D mediating TRF1 recognition and ubiquitylation.

To address whether the ubiquitylating defect observed with the FBXO4 I377M mutant results in a corresponding increase in the cyclin D1 half-life, we reconstituted Fbxo4-null MEFs with either wild-type FBXO4 or the FBXO4 I377M mutant. Although expression of wild-type FBXO4 was associated with a cyclin D1 half-life of <30 min (23), the cyclin D1 half-life remained extended in FBXO4 I377M-reconstituted cells (Fig. 6A). Similarly, melanoma cells with the endogenous *FBXO4* I377M mutant exhibited a prolonged cyclin D1 half-life (Fig. 6B). Because overexpression of cyclin D1 is associated with an increased rate of proliferation, we assessed the ability of FBXO4 and the FBXO4 I377M mutant to regulate cell proliferation in a cyclin D1-dependent manner. Indeed, while wild-type FBXO4 expression reduced the proliferation of Fbxo4-null MEFs, the FBXO4 I377M mutant was unable to suppress proliferation, consistent with its inability to regulate cyclin D1 (see Fig. S6A in the supplemental material). If the proliferative suppression associated with wild-type FBXO4 expression occurs through cyclin D1 regulation, expression of a nondegradable cyclin D1 mutant should result in cells refractory to the effects of FBXO4. Thus, we expressed FBXO4 in the presence of either wild-type cyclin D1 or a nondegradable T286A mutant. In the absence of FBXO4, wild-type cyclin D1 and the T286A mutant provided a clear growth advantage by day 6. FBXO4-containing cells suppressed growth with wild-type cyclin D1, but FBXO4 had no effect in the presence of the T286A mutation (see Fig. S6B).

To address whether the *FBXO4* I377M mutation produces a rate-limiting barrier to cyclin D1 degradation, we inhibited the proteasome to assess the potential for further cyclin D1 accumulation. In cells harboring the endogenous *FBXO4* I377M mutation, MG132 treatment failed to trigger an increase in cyclin D1 levels, whereas a striking increase was observed in wild-type *FBXO4* cells (Fig. 6C). Consistent with these results, knockdown of the Fbxo4 I377M mutant in 1205Lu cells failed to trigger increased cyclin D1 accumulation but was associated with increased Trf1 levels, while knockdown of WT FBXO4 in 451Lu cells was associated with increases in both cyclin D1 and Trf1 levels (Fig. 6D). Ectopic overexpression of the FBXO4 I377M mutant in 293T cells also resulted in higher basal cyclin D1 levels and less dramatic accumulation in response to MG132 treatment than under basal conditions (Fig. 6E). Finally, we have shown that overexpression of WT FBXO4 in mutant melanoma cells reduces cyclin D1 levels (Fig. 5D). We reasoned that this should also result in reduced growth of these

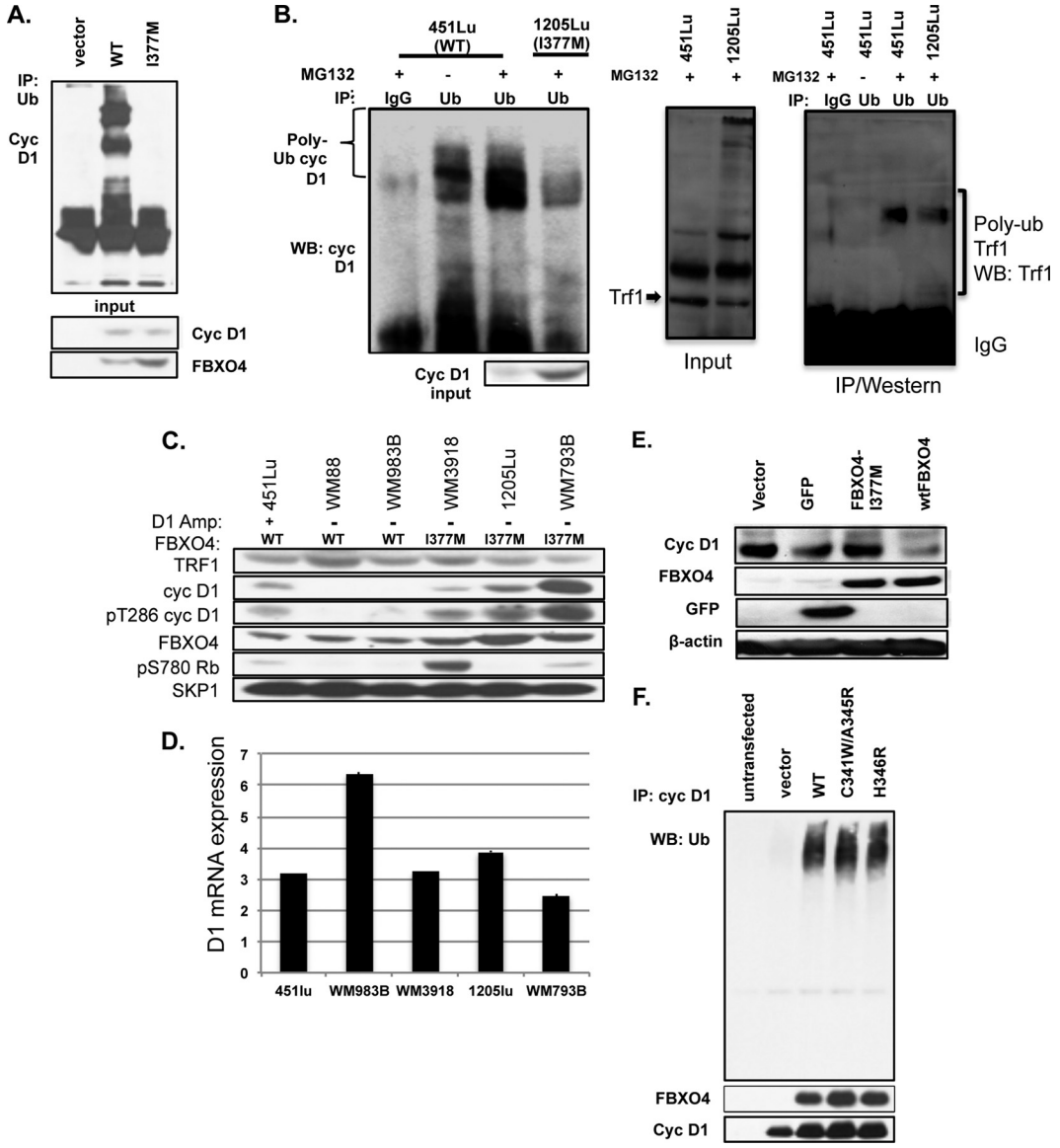


**FIG 5** The FBXO4 I377M mutant fails to regulate cyclin D1 *in vivo*. (A) Lysates from 293T cells expressing FBXO4, αB crystallin, and cyclin D1/CDK4 were immunoprecipitated for ubiquitin and blotted for polyubiquitylated cyclin D1. (B) Human melanoma 451Lu (WT FBXO4) and 1205Lu (FBXO4 I377M) cells were subjected to MG132 proteasomal inhibition and lysed, and cell extracts were immunoprecipitated for ubiquitin and immunoblotted for polyubiquitylated cyclin D1 (left) or Trf1 (right and middle). (C) Human melanoma 451Lu, WM88, WM983B, WM3918, 1205Lu, and WM793B cells (lanes 1 to 6, respectively) were lysed and analyzed by direct Western analysis for cyclin D1, pT286 cyclin D1, TRF1, FBXO4, and pS780 Rb expression. (D) Quantitative PCR for cyclin D1 mRNA from the indicated cell lines. (E) WM793B cells were infected with empty puro-pBabe-, pBabe-GFP-, WT FBXO4-, or FBXO4 I377M-containing virus and subsequently analyzed by direct Western blotting for cyclin D1, FBXO4, or GFP expression. (F) To assess the cyclin D1-ubiquitylating potential of TRF1-binding-defective mutants, FBXO4, αB crystallin, and cyclin D1/CDK4 were immunoprecipitated for cyclin D1 and probed for ubiquitylated species.

cells in soft agar, while overexpression of the FBXO4 I377M mutant should not. Indeed, a significant reduction in the number of colonies forming in soft agar was noted upon expression of WT FBXO4 (Fig. 6F). These results suggest that the FBXO4 I377M mutation presents a rate-limiting barrier to cyclin D1 regulation and oncogenic cellular proliferation.

Our current understanding of cyclin D1 oncogenic function posits that nuclear accumulation is a requisite for its transforming potential (39); we thus hypothesized that a loss of cyclin D1 surveillance would permit its nuclear localization. Wild-type FBXO4 or the FBXO4 I377M mutant was introduced into Fbxo4-null fibroblasts, and cyclin D1 localization was analyzed by immunofluorescence. FBXO4 I377M expression correlated with increased nuclear cyclin D1 accumulation, whereas cells expressing WT FBXO4 had a nearly undetectable endogenous cyclin D1 signal in the nucleus (Fig. 6G). Similarly, human melanoma cell lines retaining wild-type *FBXO4* exhibited predominantly cyclin D1 nuclear exclusion, while those containing the endogenous *FBXO4* I377M mutant failed to regulate nuclear levels (Fig. 6H; see also Fig. S7 in the supplemental material).

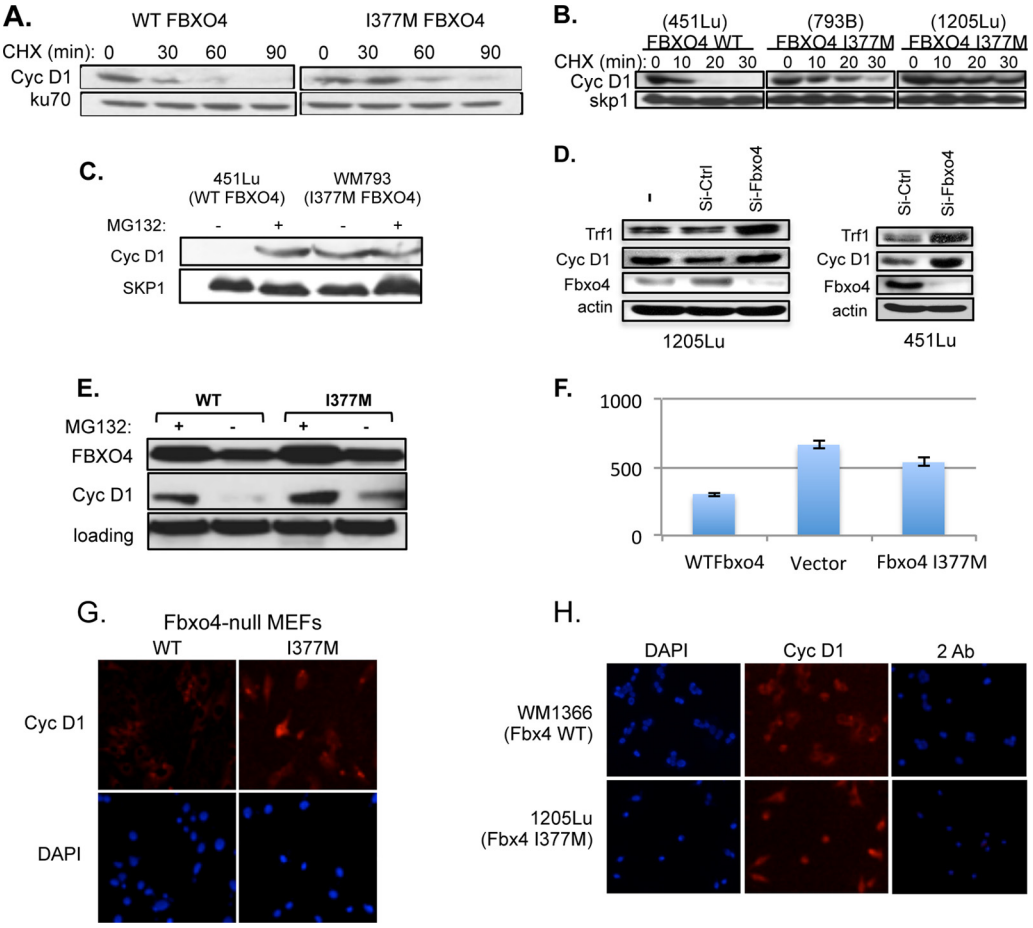


**FIG 6** Cyclin D1 turnover is defective, and nuclear accumulation occurs in the presence of the Fbxo4 I377M mutant. (A) Fbxo4-null MEFs were transiently transfected with WT FBXO4 or the FBXO4 I377M mutant, and the endogenous cyclin D1 half-life was assessed by cycloheximide (CHX) chase. (B) Human melanoma cells were treated with cycloheximide and analyzed for endogenous cyclin D1 and FBXO4 expression. (C) Human melanoma cells with or without the FBXO4 mutation were treated with or without MG132 (2 μM for 16 h) and analyzed for endogenous cyclin D1 expression. (D) Small interfering RNA (Si) Fbxo4 knockdown in 1205Lu or 451Lu cells. Immunoblotting antibodies are indicated. (E) 293T cells overexpressing WT FBXO4 or the FBXO4 I377M mutant and cyclin D1/CDK4 were treated with or without MG132 (2 μM for 16 h) and analyzed for cyclin D1 expression. (F) Cells infected with vectors encoding the indicated proteins were seeded in soft agar, and colonies were quantified after 21 days of growth. Quantifications and error bars represent results from 3 independent experiments. (G) Fbxo4-null MEFs were transiently transfected with WT FBXO4 or the FBXO4 I377M mutant, and endogenous cyclin D1 localization was analyzed by immunofluorescence. (H) Human melanoma cells with or without the FBXO4 mutation were analyzed by immunofluorescence for endogenous cyclin D1 localization.

## DISCUSSION

The critical role of cyclin D1/CDK4 in melanoma is highlighted by the frequent deletion, mutation, or promoter methylation of $p16^{INK4A}$ as well as the significant prevalence of CCND1 amplification (20, 40). In addition to these mechanisms, cyclin D1 overexpression occurs in an additional 20% of melanomas without any identifiable genetic insult, suggesting a loss of posttranslational regulation of cyclin D1 (20). We provide clinical, biochemical, and animal model evidence that inactivation of the cell cycle-regulated cyclin D1 ubiquitin ligase $SCF^{FBXO4}$ contributes to the observed dysregulation of cyclin D1 and further contributes to neoplastic growth of melanocytes *in vivo*.

Using an animal model, we provide striking evidence that *Fbxo4* suppresses $Braf^{V600E}$-driven melanoma. *Fbxo4* deficiency results in cyclin D1 accumulation. Critically, genetic *Ccnd1* deficiency protects from tumorigenesis and, importantly, does not alter the latency or penetrance of glabrous skin hyperpigmentation. These observations indicate that the downregulation of cyclin D1 in our model does not impact the melanocyte hyperproliferation associated with $Braf^{V600E}$ but does prevent neoplastic conversion. Combined with the *Fbxo4* deficiency, the wild-type *Ccnd1* gene dosage (the presence of both alleles) provides a signaling event sufficient to overcome oncogene-induced senescence, which normally suppresses tumorigenesis. Although our result suggests that the cooperation between $Braf^{V600E}$ and loss of Fbxo4 is critically dependent on cyclin D1 levels, our current study does not demonstrate that Fbxo4-mediated tumorigenesis acts solely through cyclin D1. One cannot preclude the possibility, which in fact may be very likely, that Fbxo4 also acts through other unidentified substrates to promote tumorigenesis. Specifically addressing Trf1, while some data suggest that conditional Trf1 deletion predisposes to cancer (41), a relative paucity of evidence supports the notion that Trf1 accumulation, as would be expected with Fbxo4 deletion, contributes to malignancy. Furthermore, the fact that murine telomeres are greatly extended and dissimilar to human telomeres further argues against telo-

mere maintenance as a contributing factor. Taken together, these results establish that cyclin D1 dose escalation is a critical mediator of malignant transformation in $Braf^{V600E}$ melanomas in the setting of Fbxo4 deficiency.

We found that the solvent-accessible *FBXO4* I377M mutation occurred in 8% of the human melanoma samples screened. It is possible that the true incidence of the I377M mutation is lower than what we observed, in light of the absence of detectable FBXO4 mutations in several other screens (42, 43). Furthermore, the somatic nature of the I377M mutation is unknown. Two instances of the *FBXO4* I377M mutation have been reported in the Single Nucleotide Polymorphism database: 1/4,512 alleles (0.0002%) in 1000Genomes and 1/9,100 alleles (0.0001%) in ESP4500. Thus, while the allele has been observed in the germ line, it is extremely rare and cannot account for the frequency seen in this study.

While the frequency of the I377M mutation in melanoma is lower than those of mutations in FBXO4 observed in cancers of the esophagus, the characterization of the biochemical effect of the mutation has provided striking insights into Fbxo4 function. Analysis of the I377M mutation has provided insights into FBXO4 substrate recognition. To date, two Fbxo4 substrates have been reported, cyclin D1 and TRF1, the latter being a component of the shelterin complex that regulates telomere stability (38, 41, 44). We highlight several lines of evidence that indicate that dysregulated cyclin D1, as opposed to TRF1, mediates the tumorigenic phenotype that we observed. The *FBXO4* I377M mutant identified from clinical data, residing within α-helix E, retains a full capacity to recruit TRF1 for ubiquitylation. The location of this mutation is in contrast to the residues within α-helix D (residues 341 to 352), which have been shown to be critical for TRF1 binding/ubiquitylation (37). Combined with our observation that the FBXO4 I377M mutant is cyclin D1 binding/ubiquitylation deficient, these data imply that there exists distinct substrate interfaces within the Fbxo4 substrate-binding domain. With regard to substrate selectivity, compared to cyclin D1, few existing lines of evidence support the notion that TRF1 dysregulation, particularly accumulation, leads to tumorigenesis. More importantly, TRF1 dysregulation was not observed in *FBXO4* mutant cells, precluding TRF1 degradation-related effects on tumorigenesis. Finally, we previously demonstrated that Fbxo4 deficiency accelerates cellular transformation *in vitro* and that this effect was critically dependent on cyclin D1, as MEFs nullizygous for cyclin D1 lost their transforming capacity (28).

The selective impact of the I377M mutation on cyclin D1 may explain why no truncating mutations in FBXO4 have been observed; the concomitant dysregulation of one substrate with the preserved regulation of another substrate(s) may provide an optimal oncogenic hit. This interpretation lays the foundation for a novel paradigm wherein SCF ubiquitin ligases may differentially regulate multiple substrates and helps explain why certain mutations may be selected in cancer. While similar to *FBXW7* in that hemizygous mutations in human cancers lead to impaired substrate regulation, Fbxo4 lacks the multiple proto-oncogenic substrates of Fbw7 (e.g., c-myc, cyclin E, and c-Jun) (45–49), thus providing an explanation for the observation that the only observed *FBXO4* mutations were missense mutations, perhaps a mechanism for selective substrate regulation.

Our *in vivo* melanoma model using $Braf^{V600E}$ on an Fbxo4-deleted background provides striking support for the role of FBXO4 in opposing neoplastic transformation of melanocytes. Thus, while cyclin D1/CDK4 dysregulation through $p16^{INK4A}$ inactivation has been known to be a major event in the development of melanoma, the current work reveals an unappreciated role for FBXO4 in melanocyte proliferative homeostasis. Additional F-box family members have been implicated in the regulation of cyclin D1 degradation, including FBXW8, FBXO31, APC/C, and SKP2 (50–53). We have also sequenced the genes encoding FBXW8 and FBXO31 in 15 primary melanoma cell lines. For *FBXW8*, only known polymorphisms were noted. For *FBXO31*, no variants were noted. We also evaluated the genes for mutations in the Cancer Genome Atlas data by using cBioPortal (http://www.cbioportal.org/). In 225 samples, two (0.8%) missense mutations were found in *FBXO31*, one with a low predicted functional impact and one with a moderate predicted functional impact (but present in only 5% of alleles). In *FBXW8*, only one (0.4%) missense mutation with a predicted moderate effect was found. Together, these data do not suggest a role for mutations in *FBXO31* and *FBXW8* in melanoma.

A recent independent investigation has called for a reevaluation of the role of F-box proteins in cyclin D1 degradation. Recently, the contributions of the E3 ligases suggested to regulate cyclin D1 have been questioned, and it was suggested that none were required for regulation of cyclin D1 degradation (54). Importantly, while ubiquitin-mediated cyclin D1 turnover was observed in the context of Fbxo4 deletion, we have rigorously demonstrated Fbxo4-dependent cyclin D1 stabilization and tumorigenesis in mice and in multiple cancer and noncancerous cell types. In this context, Fbxo4 specifically catalyzes the removal of cyclin D1 beginning at the $G_1$/S-phase transition, thereby preventing nuclear accumulation during S phase. Thus, Fbxo4 governs cyclin D1 accumulation during this critical phase of the cell cycle, since prolonged nuclear CDK4 activity through S phase drives DNA rereplication, resulting in genomic instability (26, 27).

In summary, our data reveal that Fbxo4, the E3 ligase for cyclin D1, is subject to inactivating mutations in melanoma. Strikingly, one of the mutations identified specifically disrupts Fbxo4-dependent regulation of cyclin D1 while retaining its ability to regulate Trf1. The bona fide tumor suppressor activity of Fbxo4 as well as its relationship with cyclin D1 were established by genetically intercrossing a model of inducible somatic $Braf^{V600E}$ mutations with *Fbxo4*-deficient mice. These mice develop rapidly progressing melanoma with a 6-week latency, and melanoma development is critically dependent on cyclin D1 levels. These findings support a role for Fbxo4 as a tumor suppressor in melanoma and provide novel insights into Fbxo4 substrate regulation. Future studies investigating the role of Fbxo4 in an array of human malignancies, how mutational status may portend a better or worse prognosis, as well as methods to counteract Fbxo4 inactivation, such as CDK inhibition, are warranted.

## ACKNOWLEDGMENTS

We thank Trish Brafford of The Wistar Institute for melanoma cell lines and guidance; Keith Flaherty, Patricia Van Belle, and David Elder for assistance in tumor collection; Xuedong Liu for anti-TRF1 serum; and Madhavi Vaddi at the Penn Genomics Facility, Quian-Chen Yu, the Histology Core Facility, and the Animal Core Facility for excellent technical assistance.

The work was supported by the Abramson Cancer Center at the Uni-

versity of Pennsylvania and National Institutes of Health grants CA133154, R25 CA101871-07, and P50CA093372. Services provided in the Penn Genomics Facility are supported by Abramson Cancer Center core grant 5P30CA016520.

## REFERENCES


1. **Chin L.** 2003. The genetics of malignant melanoma: lessons from mouse and man. Nat. Rev. Cancer **3:**559–570.
2. **Chin L, Merlino G, DePinho RA.** 1998. Malignant melanoma: modern black plague and genetic black box. Genes Dev. **12:**3467–3481.
3. **Davies H, Bignell GR, Cox C, Stephens P, Edkins S, Clegg S, Teague J, Woffendin H, Garnett MJ, Bottomley W, Davis N, Dicks E, Ewing R, Floyd Y, Gray K, Hall S, Hawes R, Hughes J, Kosmidou V, Menzies A, Mould C, Parker A, Stevens C, Watt S, Hooper S, Wilson R, Jayatilake H, Gusterson BA, Cooper C, Shipley J, Hargrave D, Pritchard-Jones K, Maitland N, Chenevix-Trench G, Riggins GJ, Bigner DD, Palmieri G, Cossu A, Flanagan A, Nicholson A, Ho JW, Leung SY, Yuen ST, Weber BL, Seigler HF, Darrow TL, Paterson H, Marais R, Marshall CJ, Wooster R, Stratton MR, Futreal PA.** 2002. Mutations of the BRAF gene in human cancer. Nature **417:**949–954.
4. **Pollock PM, Harper UL, Hansen KS, Yudt LM, Stark M, Robbins CM, Moses TY, Hostetter G, Wagner U, Kakareka J, Salem G, Pohida T, Heenan P, Duray P, Kallioniemi O, Hayward NK, Trent JM, Meltzer PS.** 2003. High frequency of BRAF mutations in nevi. Nat. Genet. **33:**19–20.
5. **Chapman PB, Hauschild A, Robert C, Haanen JB, Ascierto P, Larkin J, Dummer R, Garbe C, Testori A, Maio M, Hogg D, Lorigan P, Lebbe C, Jouary T, Schadendorf D, Ribas A, O'Day SJ, Sosman JA, Kirkwood JM, Eggermont AM, Dreno B, Nolop K, Li J, Nelson B, Hou J, Lee RJ, Flaherty KT, McArthur GA.** 2011. Improved survival with vemurafenib in melanoma with BRAF V600E mutation. N. Engl. J. Med. **364:**2507–2516.
6. **Flaherty KT, Puzanov I, Kim KB, Ribas A, McArthur GA, Sosman JA, O'Dwyer PJ, Lee RJ, Grippo JF, Nolop K, Chapman PB.** 2010. Inhibition of mutated, activated BRAF in metastatic melanoma. N. Engl. J. Med. **363:**809–819.
7. **Sosman JA, Kim KB, Schuchter L, Gonzalez R, Pavlick AC, Weber JS, McArthur GA, Hutson TE, Moschos SJ, Flaherty KT, Hersey P, Kefford R, Lawrence D, Puzanov I, Lewis KD, Amaravadi RK, Chmielowski B, Lawrence HJ, Shyr Y, Ye F, Li J, Nolop KB, Lee RJ, Joe AK, Ribas A.** 2012. Survival in BRAF V600-mutant advanced melanoma treated with vemurafenib. N. Engl. J. Med. **366:**707–714.
8. **Dankort D, Curley DP, Cartlidge RA, Nelson B, Karnezis AN, Damsky WE, Jr, You MJ, DePinho RA, McMahon M, Bosenberg M.** 2009. Braf(V600E) cooperates with Pten loss to induce metastatic melanoma. Nat. Genet. **41:**544–552.
9. **Gray-Schopfer VC, Cheong SC, Chong H, Chow J, Moss T, Abdel-Malek ZA, Marais R, Wynford-Thomas D, Bennett DC.** 2006. Cellular senescence in naevi and immortalisation in melanoma: a role for p16? Br. J. Cancer **95:**496–505.
10. **Michaloglou C, Vredeveld LC, Soengas MS, Denoyelle C, Kuilman T, van der Horst CM, Majoor DM, Shay JW, Mooi WJ, Peeper DS.** 2005. BRAFE600-associated senescence-like cell cycle arrest of human naevi. Nature **436:**720–724.
11. **Ackermann J, Frutschi M, Kaloulis K, McKee T, Trumpp A, Beermann F.** 2005. Metastasizing melanoma formation caused by expression of activated N-RasQ61K on an INK4a-deficient background. Cancer Res. **65:**4005–4011.
12. **Bennecke M, Kriegl L, Bajbouj M, Retzlaff K, Robine S, Jung A, Arkan MC, Kirchner T, Greten FR.** 2010. Ink4a/Arf and oncogene-induced senescence prevent tumor progression during alternative colorectal tumorigenesis. Cancer Cell **18:**135–146.
13. **Dhomen N, Reis-Filho JS, da Rocha Dias S, Hayward R, Savage K, Delmas V, Larue L, Pritchard C, Marais R.** 2009. Oncogenic Braf induces melanocyte senescence and melanoma in mice. Cancer Cell **15:**294–303.
14. **Ferguson B, Konrad Muller H, Handoko HY, Khosrotehrani K, Beermann F, Hacker E, Soyer HP, Bosenberg M, Walker GJ.** 2010. Differential roles of the pRb and Arf/p53 pathways in murine naevus and melanoma genesis. Pigment Cell Melanoma Res. **23:**771–780.
15. **Goel VK, Ibrahim N, Jiang G, Singhal M, Fee S, Flotte T, Westmoreland S, Haluska FS, Hinds PW, Haluska FG.** 2009. Melanocytic nevus-like hyperplasia and melanoma in transgenic BRAFV600E mice. Oncogene **28:**2289–2298.
16. **Kannan K, Sharpless NE, Xu J, O'Hagan RC, Bosenberg M, Chin L.** 2003. Components of the Rb pathway are critical targets of UV mutagenesis in a murine melanoma model. Proc. Natl. Acad. Sci. U. S. A. **100:**1221–1225.
17. **Sviderskaya EV, Hill SP, Evans-Whipp TJ, Chin L, Orlow SJ, Easty DJ, Cheong SC, Beach D, DePinho RA, Bennett DC.** 2002. p16(Ink4a) in melanocyte senescence and differentiation. J. Natl. Cancer Inst. **94:**446–454.
18. **Ibrahim N, Haluska FG.** 2009. Molecular pathogenesis of cutaneous melanocytic neoplasms. Annu. Rev. Pathol. **4:**551–579.
19. **Weisenberger DJ, Siegmund KD, Campan M, Young J, Long TI, Faasse MA, Kang GH, Widschwendter M, Weener D, Buchanan D, Koh H, Simms L, Barker M, Leggett B, Levine J, Kim M, French AJ, Thibodeau SN, Jass J, Haile R, Laird PW.** 2006. CpG island methylator phenotype underlies sporadic microsatellite instability and is tightly associated with BRAF mutation in colorectal cancer. Nat. Genet. **38:**787–793.
20. **Sauter ER, Yeo UC, von Stemm A, Zhu W, Litwin S, Tichansky DS, Pistritto G, Nesbit M, Pinkel D, Herlyn M, Bastian BC.** 2002. Cyclin D1 is a candidate oncogene in cutaneous melanoma. Cancer Res. **62:**3200–3206.
21. **Diehl JA, Zindy F, Sherr CJ.** 1997. Inhibition of cyclin D1 phosphorylation on threonine-286 prevents its rapid degradation via the ubiquitin-proteasome pathway. Genes Dev. **11:**957–972.
22. **Lin DI, Barbash O, Kumar KG, Weber JD, Harper JW, Klein-Szanto AJ, Rustgi A, Fuchs SY, Diehl JA.** 2006. Phosphorylation-dependent ubiquitination of cyclin D1 by the SCF(FBX4-alphaB crystallin) complex. Mol. Cell **24:**355–366.
23. **Vaites LP, Lee EK, Lian Z, Barbash O, Roy D, Wasik M, Klein-Szanto AJ, Rustgi AK, Diehl JA.** 2011. The Fbx4 tumor suppressor regulates cyclin D1 accumulation and prevents neoplastic transformation. Mol. Cell. Biol. **31:**4513–4523.
24. **Deshaies RJ, Joazeiro CA.** 2009. RING domain E3 ubiquitin ligases. Annu. Rev. Biochem. **78:**399–434.
25. **Silverman JS, Skaar JR, Pagano M.** 2012. SCF ubiquitin ligases in the maintenance of genome stability. Trends Biochem. Sci. **37:**66–73.
26. **Aggarwal P, Lessie MD, Lin DI, Pontano L, Gladden AB, Nuskey B, Goradia A, Wasik MA, Klein-Szanto AJ, Rustgi AK, Bassing CH, Diehl JA.** 2007. Nuclear accumulation of cyclin D1 during S phase inhibits Cul4-dependent Cdt1 proteolysis and triggers p53-dependent DNA rereplication. Genes Dev. **21:**2908–2922.
27. **Aggarwal P, Vaites LP, Kim JK, Mellert H, Gurung B, Nakagawa H, Herlyn M, Hua X, Rustgi AK, McMahon SB, Diehl JA.** 2010. Nuclear cyclin D1/CDK4 kinase regulates CUL4 expression and triggers neoplastic growth via activation of the PRMT5 methyltransferase. Cancer Cell **18:**329–340.
28. **Barbash O, Zamfirova P, Lin DI, Chen X, Yang K, Nakagawa H, Lu F, Rustgi AK, Diehl JA.** 2008. Mutations in Fbx4 inhibit dimerization of the SCF(Fbx4) ligase and contribute to cyclin D1 overexpression in human cancer. Cancer Cell **14:**68–78.
29. **Korcheva VB, Levine J, Beadling C, Warrick A, Countryman G, Olson NR, Heinrich MC, Corless CL, Troxell ML.** 2011. Immunohistochemical and molecular markers in breast phyllodes tumors. Appl. Immunohistochem. Mol. Morphol. **19:**119–125.
30. **Bradford MM.** 1976. A rapid and sensitive method for the quantitation of microgram quantities of protein utilizing the principle of protein-dye binding. Anal. Biochem. **72:**248–254.
31. **Dankort D, Filenova E, Collado M, Serrano M, Jones K, McMahon M.** 2007. A new mouse model to explore the initiation, progression, and therapy of BRAFV600E-induced lung tumors. Genes Dev. **21:**379–384.
32. **Sicinski P, Donaher JL, Parker SB, Li T, Fazeli A, Gardner H, Haslam SZ, Bronson RT, Elledge SJ, Weinberg RA.** 1995. Cyclin D1 provides a link between development and oncogenesis in the retina and breast. Cell **82:**621–630.
33. **Cochran AJ, Lu HF, Li PX, Saxton R, Wen DR.** 1993. S-100 protein remains a practical marker for melanocytic and other tumours. Melanoma Res. **3:**325–330.
34. **Magro CM, Crowson AN, Mihm MC.** 2006. Unusual variants of malignant melanoma. Mod. Pathol. **19**(Suppl 2)**:**S41–S70. doi:10.1038/modpathol.3800516.
35. **Li Y, Hao B.** 2010. Structural basis of dimerization-dependent ubiquiti-

nation by the SCF(Fbx4) ubiquitin ligase. J. Biol. Chem. **285:**13896–13906.
36. **Barbash O, Lee EK, Diehl JA.** 2010. Phosphorylation-dependent regulation of SCF(Fbx4) dimerization and activity involves a novel component, 14-3-3epsilon. Oncogene **30:**1995–2002.
37. **Zeng Z, Wang W, Yang Y, Chen Y, Yang X, Diehl JA, Liu X, Lei M.** 2010. Structural basis of selective ubiquitination of TRF1 by SCFFbx4. Dev. Cell **18:**214–225.
38. **Lee TH, Perrem K, Harper JW, Lu KP, Zhou XZ.** 2006. The F-box protein FBX4 targets PIN2/TRF1 for ubiquitin-mediated degradation and regulates telomere maintenance. J. Biol. Chem. **281:**759–768.
39. **Alt JR, Cleveland JL, Hannink M, Diehl JA.** 2000. Phosphorylation-dependent regulation of cyclin D1 nuclear export and cyclin D1-dependent cellular transformation. Genes Dev. **14:**3102–3114.
40. **Palmieri G, Capone M, Ascierto ML, Gentilcore G, Stroncek DF, Casula M, Sini MC, Palla M, Mozzillo N, Ascierto PA.** 2009. Main roads to melanoma. J. Transl. Med. **7:**86. doi:10.1186/1479-5876-7-86.
41. **Martinez P, Thanasoula M, Munoz P, Liao C, Tejera A, McNees C, Flores JM, Fernandez-Capetillo O, Tarsounas M, Blasco MA.** 2009. Increased telomere fragility and fusions resulting from TRF1 deficiency lead to degenerative pathologies and increased cancer in mice. Genes Dev. **23:**2060–2075.
42. **Berger MF, Hodis E, Heffernan TP, Deribe YL, Lawrence MS, Protopopov A, Ivanova E, Watson IR, Nickerson E, Ghosh P, Zhang H, Zeid R, Ren X, Cibulskis K, Sivachenko AY, Wagle N, Sucker A, Sougnez C, Onofrio R, Ambrogio L, Auclair D, Fennell T, Carter SL, Drier Y, Stojanov P, Singer MA, Voet D, Jing R, Saksena G, Barretina J, Ramos AH, Pugh TJ, Stransky N, Parkin M, Winckler W, Mahan S, Ardlie K, Baldwin J, Wargo J, Schadendorf D, Meyerson M, Gabriel SB, Golub TR, Wagner SN, Lander ES, Getz G, Chin L, Garraway LA.** 2012. Melanoma genome sequencing reveals frequent PREX2 mutations. Nature **485:**502–506.
43. **Hodis E, Watson IR, Kryukov GV, Arold ST, Imielinski M, Theurillat JP, Nickerson E, Auclair D, Li L, Place C, Dicara D, Ramos AH, Lawrence MS, Cibulskis K, Sivachenko A, Voet D, Saksena G, Stransky N, Onofrio RC, Winckler W, Ardlie K, Wagle N, Wargo J, Chong K, Morton DL, Stemke-Hale K, Chen G, Noble M, Meyerson M, Ladbury JE, Davies MA, Gershenwald JE, Wagner SN, Hoon DS, Schadendorf D, Lander ES, Gabriel SB, Getz G, Garraway LA, Chin L.** 2012. A landscape of driver mutations in melanoma. Cell **150:**251–263.
44. **Zhou XZ, Perrem K, Lu KP.** 2003. Role of Pin2/TRF1 in telomere maintenance and cell cycle control. J. Cell. Biochem. **89:**19–37.
45. **Knuutila S, Aalto Y, Autio K, Bjorkqvist AM, El-Rifai W, Hemmer S, Huhta T, Kettunen E, Kiuru-Kuhlefelt S, Larramendy ML, Lushnikova T, Monni O, Pere H, Tapper J, Tarkkanen M, Varis A, Wasenius VM, Wolf M, Zhu Y.** 1999. DNA copy number losses in human neoplasms. Am. J. Pathol. **155:**683–694.
46. **Nakayama KI, Nakayama K.** 2006. Ubiquitin ligases: cell-cycle control and cancer. Nat. Rev. Cancer **6:**369–381.
47. **Song JH, Schnittke N, Zaat A, Walsh CS, Miller CW.** 2008. FBXW7 mutation in adult T-cell and B-cell acute lymphocytic leukemias. Leuk. Res. **32:**1751–1755.
48. **Spruck CH, Strohmaier H, Sangfelt O, Muller HM, Hubalek M, Muller-Holzner E, Marth C, Widschwendter M, Reed SI.** 2002. hCDC4 gene mutations in endometrial cancer. Cancer Res. **62:**4535–4539.
49. **Welcker M, Clurman BE.** 2008. FBW7 ubiquitin ligase: a tumour suppressor at the crossroads of cell division, growth and differentiation. Nat. Rev. Cancer **8:**83–93.
50. **Okabe H, Lee SH, Phuchareon J, Albertson DG, McCormick F, Tetsu O.** 2006. A critical role for FBXW8 and MAPK in cyclin D1 degradation and cancer cell proliferation. PLoS One **1:**e128. doi:10.1371/journal.pone.0000128.
51. **Pawar SA, Sarkar TR, Balamurugan K, Sharan S, Wang J, Zhang Y, Dowdy SF, Huang AM, Sterneck E.** 2010. C/EBPdelta targets cyclin D1 for proteasome-mediated degradation via induction of CDC27/APC3 expression. Proc. Natl. Acad. Sci. U. S. A. **107:**9210–9215.
52. **Santra MK, Wajapeyee N, Green MR.** 2009. F-box protein FBXO31 mediates cyclin D1 degradation to induce G1 arrest after DNA damage. Nature **459:**722–725.
53. **Yu ZK, Gervais JL, Zhang H.** 1998. Human CUL-1 associates with the SKP1/SKP2 complex and regulates p21(CIP1/WAF1) and cyclin D proteins. Proc. Natl. Acad. Sci. U. S. A. **95:**11324–11329.
54. **Kanie T, Onoyama I, Matsumoto A, Yamada M, Nakatsumi H, Tateishi Y, Yamamura S, Tsunematsu R, Matsumoto M, Nakayama KI.** 2012. Genetic reevaluation of the role of F-box proteins in cyclin D1 degradation. Mol. Cell. Biol. **32:**590–605.